first dynode, the entire multiplier was isolated completely from earth ground, and the first dynode was connected directly to the electrometer. The metallic cylinder containing the multiplier was biased with a negative potential with respect to the multiplier. The same electrometer that was used to measure the ion current in the collision chamber was used with the multiplier. However, as shown in Fig. 2, the transmission ratio measured was always $1.1 < T < 1.2$ for "100%" transmission. This indicates that secondary electron suppression was not as good in the electron multiplier measurement as it was in the collision chamber.

[15]A. Papoulis, *Systems and Transforms with Applications in Optics* (McGraw-Hill, New York, 1968).

[16]P. A. Sturrock, *Static and Dynamic Electron Optics* (Cambridge U.P., Cambridge, 1955).

[17]S. Ruthberg, Natl. Bur. Std. (private communication).

[18]W. H. Cramer, J. Chem. Phys. 35, 836 (1961).

[19]D. W. Koopman, Phys. Rev. 154, 79 (1967).

[20]E. W. McDaniel, *Collisional Phenomena in Ionized Gases* (Wiley, New York, 1964).

[21]H. Udseth, C. F. Giese, and W. R. Gentry, J. Chem. Phys. 54, 3642 (1971).

[22]The relation $\chi_r = B(\epsilon/E)$ has been found to be valid on the basis of theoretical and experimental evidence for $\chi_r \lesssim 90°$. Furthermore, it is quite evident that the constant B is relatively insensitive to changes in the interaction well depth ϵ, and that with χ_r in degrees, the constant $B \simeq 115 \pm 15$ for both ion-neutral and neutral-neutral interactions. For theoretical results on χ_r, see E. A. Mason, J. Chem. Phys. 26, 667 (1957), and E. A. Mason, R. J. Munn, and F. J. Smith, J. Chem. Phys. 44, 1967 (1966). For experimental results on ion-neutral interactions, see F. A. Herrero, E. M. Nemeth, and T. L. Bailey, J. Chem. Phys. 50, 4591 (1969), and R. L. Champion *et al.*, Phys. Rev. A 2, 2327 (1970). For experimental results on neutral-neutral interactions, see F. A. Morse and R. B. Bernstein, J. Chem. Phys. 37, 2019 (1962), and D. Beck, J. Chem. Phys. 37, 2884 (1962). Adopting a value of $B = 115$, we obtain $\epsilon \simeq 2$ eV for the average well depth of the anisotropic interaction of H^+-H_2.

[23]J. H. Moore, Jr. and J. P. Doering, Phys. Rev. 174, 178 (1968).

[24]J. Korobkin and Z. I. Slawsky, J. Chem. Phys. 37, 226 (1962).

[25]F. W. DeWette and Z. I. Slawsky, Physics 20, 1169 (1954).

[26]H. S. W. Massey, Rept. Progr. Phys. 12, 248 (1948–49); E. Gerjuoy, Rev. Mod. Phys. 33, 544 (1961).

[27]K. W. Ford and J. A. Wheeler, Ann. Phys. (N.Y.) 7, 259 (1959).

PHYSICAL REVIEW A VOLUME 5, NUMBER 2 FEBRUARY 1972

Measurements of Energy and Angular Distributions of Secondary Electrons Produced in Electron-Impact Ionization of Helium*

W. K. Peterson,† E. C. Beaty,‡ and C. B. Opal§
Joint Institute for Laboratory Astrophysics, University of Colorado, Boulder, Colorado 80302
(Received 27 September 1971)

The energy and angular distributions of electrons produced in the ionization of helium by electrons with energies between 100 eV and 2 keV have been measured in a crossed-beam apparatus consisting of a fixed hemispherical energy analyzer and a rotatable electron gun. Distributions of secondary electrons (those electrons departing with energies less than one-half that of the incident primary electrons) were obtained for a wide range of energies and for angles between 30° and 150° with respect to the direction of the incident primary electron beam. The observed angular distributions were significantly different from the results of two early electron-impact measurements; however, they agreed to the extent expected with more recent results and with similar proton-impact data. For secondary energies above about 50 eV and for primary energies greater than 300 eV, the energy distributions (the cross sections integrated over angle) were observed to be very nearly equal to the distribution given by the Mott formula for free-electron–free-electron scattering multiplied by the number of electrons in the target.

I. INTRODUCTION

Cross sections for the production of low-energy electrons ejected in electron-impact ionization by fast electrons are of importance in plasma physics, atmospheric physics, and radiation chemistry. In particular, since electron-impact excitation and ionization cross sections are largest in the energy range 20–200 eV for most atomic and molecular species, knowledge of the rate of production of secondary electrons in this energy range by high-energy electron-impact ionization is essential to an understanding of the total energy deposition by fast particles. Relatively little has been published about these cross sections. In a previous short note,[1] we reported measurements of the energy distribution of secondary electrons produced in electron-impact ionization of helium and compared the results to Born-approximation calculations. In this paper we give a more complete account of the experimental procedure and discuss in greater detail the observed energy and angular distributions.[2]

The quantity we have measured is the doubly differential cross section [called $\sigma(E_p, E_s, \theta)$ and ex-

pressed in units of $cm^2/eV\,sr$] for emission of an electron of energy E_s at an angle θ with respect to the incident primary electron of energy E_p. The helium atom is sufficiently simple that it is reasonable to expect to be able to understand the ionization process in terms of a complete quantum-mechanical description. Fortunately, of the processes involving both the electrons in the He atom—ionization to excited states[3] of He^+, double excitation followed by autoionization (discussed below), and double ionization[4]—no one contributes more than 1% of the total ionization cross section. Although the data include all processes, for purposes of discussion we shall assume that only the simple process of direct ionization to the ground states of He^+ has occurred. It is worth noting that two-electron processes are relatively more important in more complicated atoms and molecules and that therefore much of the discussion below should be modified before application to such atoms or molecules.

Because of the large mass ratio, the kinetic energy imparted to the ion in the ionization process is negligible, and the energies of the two departing electrons must sum to $E_p - I$, where I is the ionization potential (24.6 eV). If the momentum imparted to the ion were also negligible, the angle between the directions of the two departing electrons would be well defined (90° if I were zero). Thus if either electron were detected, the energy and angle of the other could be determined and it would be possible to predict $\sigma(E_p, E_s, \theta)$ for $E_s < \frac{1}{2}(E_p - I)$ from measurements of the cross section for $E_s > \frac{1}{2}(E_p - I)$ and vice versa. However, because the ion can in fact carry away an appreciable amount of momentum, the directions of the two departing electrons are not highly correlated. More information than is given by $\sigma(E_p, E_s, \theta)$ is necessary in order to define completely the ionization process. This information could be obtained, for example, by observing the two departing electrons in coincidence. Ehrhart *et al.*[5] have made such measurements for a limited range of the relevant variables. If sufficient data of this sort were available, $\sigma(E_p, E_s, \theta)$ could be derived by summing over the energy and angle of the high-energy electrons.

By summing the departing electron spectrum over angle, one obtains the singly differential cross section

$$\sigma(E_p, E_s) = \int_0^{\pi} \sigma(E_p, E_s, \theta)\, 2\pi \sin\theta\, d\theta \qquad (1)$$

(in cm^2/eV), which indeed is symmetrical about $\frac{1}{2}(E_p - I)$ regardless of the momentum transfered to the ion. However, available quantitative measurements of the doubly differential cross section in the upper-half of the spectrum[6] (the "energy-loss" or "degraded-primary" spectrum) do not yet include a large enough energy loss and angular range to allow one to compute the entire singly differential spectrum.[7] Until recently, the only data available on the lower-half of the spectrum (which we shall call the "ejected" or "secondary" electron spectrum) were the results of some early work[8,9] which are of doubtful validity. Since the publication of our short note,[1] some additional data on the secondary spectrum of helium have become available.[10,11]

In view of the lack of complete and reliable data on the low-energy part of the spectrum and because of its importance in energy-degradation studies, the apparatus was designed to be optimum for studying $\sigma(E_p, E_s, \theta)$ for $E_s < \frac{1}{2}(E_p - I)$.

II. APPARATUS AND EXPERIMENTAL PROCEDURE

The crossed-beam apparatus is illustrated in Fig. 1. Secondary electrons from the intersection of an electron beam, produced in a rotatable electron gun (1), with an atomic beam produced by admitting the target gas through a small tube (10), were collected by the input electron optics (2) and focused onto the entrance plane of the hemispherical analyzer (3). A small part of the dispersed spectrum was then refocused by the output optics (4) through an exit slit (5) onto a channel electron multiplier (6). Standard nuclear pulse counting electronics were used to process the signal. Extensive shielding was used to discriminate against the low-energy electrons which were not produced in the interaction region.

Recent measurements of cross sections for the production of secondary electrons by proton impact[12,13] show that there is little structure in either the energy or the angular distributions of the secondary electrons. Since there was reason to expect similar results for electron impact, the experimental design featured low angular and energy resolution and wide dynamic range. With the apertures and slits used in the present measurements, the acceptance angle of the analyzer was about 15° and the energy resolution ($\Delta E/E$) was about 10%.

A. Energy Analyzer and Electron Optics

The electron optics and hemispherical analyzer were of standard design.[14] The relatively broad energy resolution chosen for this measurement meant that the hemispheres did not have to be machined from a solid piece of stock to close tolerances. Instead, hemispherical shells (with nominal diameters of 10 and 15 cm) pressed from No. 304 stainless steel were obtained commercially. A lens spherometer showed them to be spherical within 1 mm ($\Delta r/r \approx 0.01$). The other elements of the analyzer were machined from No. 304 stainless steel to a tolerance of ~0.03 mm. Alignment of the analyzer was achieved with mechanical constraints machined into the apparatus. To reduce the effects of contact potential differences and secondary electron production, all inside surfaces of the analyzer and

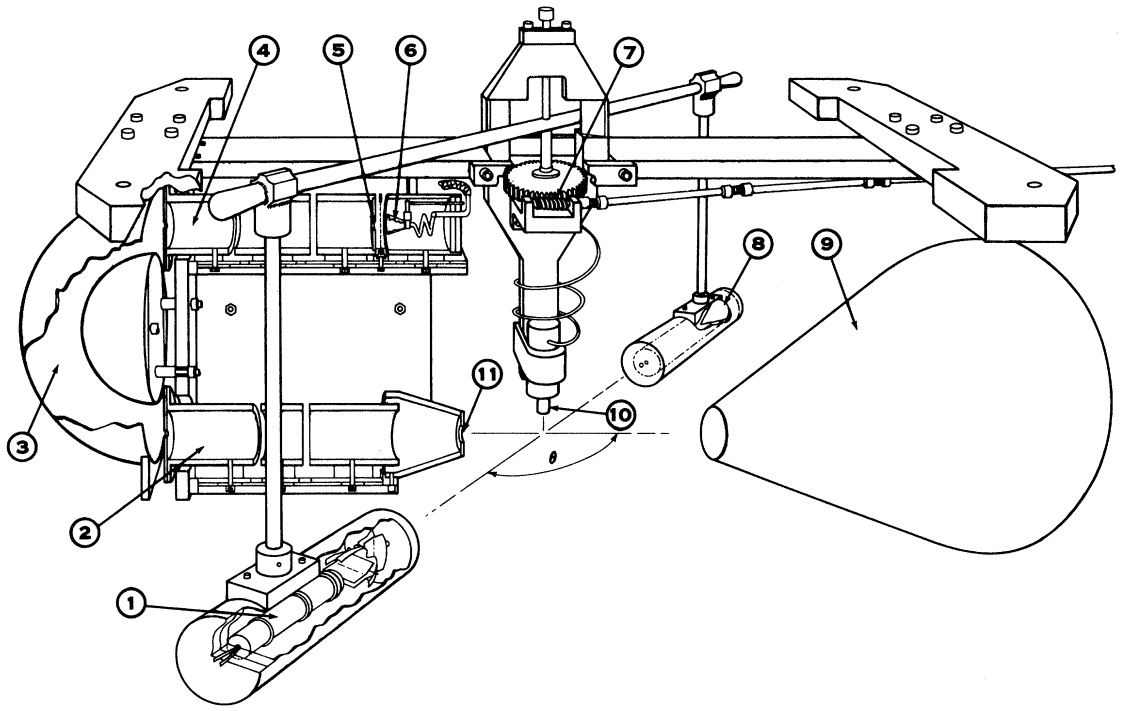

FIG. 1. Apparatus: 1, electron gun; 2, input lenses; 3, hemispherical analyzer; 4, output lenses; 5, exit slit; 6, detector; 7, angle drive; 8, Faraday cup; 9, conical trap; 10, gas supply; 11, limiting aperture.

lenses were gold blacked. All parts made of No. 304 stainless steel were vacuum annealed to eliminate surface magnetic fields created in machining operations. The earth's magnetic field was nulled (to less than 5 mG) by three orthogonal sets of 1.3-m-diam Helmholtz coils. Alternating 60-Hz magnetic fields were observed to be approximately 7 mG (peak to peak) at the interaction region.

The angular acceptance of the analyzer was made as large as practical in order to obtain a large signal. The large angular acceptance led to large filling factors in the electron lens elements (the calculated maximum was 0.8). Because of the uncertainties in the electron optical properties and the aberrations associated with large filling factors, the effective angular acceptance could not be calculated exactly; we estimate that the acceptance was about 15° for the data reported here. With the exit slit used, the energy resolution of the analyzer was calculated to be 4%, and measured to be 9%. The difference is attributed to the lack of a sharp image formed by the electron optics.

The energy E_s passed by the analyzer was selected by driving all the lens elements and analyzer plates from a common power supply through resistive dividers. The potential of the common power supply was proportional to the energy E_s. This mode of operation was used to take advantage of the fact that the electron optical properties of electrostatic lenses and analyzers depend only on voltage ratios. The sensitivity of the analyzer-lens system to monochromatic electrons was therefore nominally independent of the energy E_s of the electrons being analyzed. In practice, second-order effects such as residual magnetic fields and contact potentials became important for low electron energies and set the lower limit to the energies studied here (4 eV).

The characteristic problem in making measurements of the type reported here arises from spurious secondary electrons produced on surfaces. Several features were incorporated in the design of the analyzer to reduce such effects. The analyzer and its electron optics were enclosed in sheet-metal shields to prevent these electrons from entering the analyzer except through the entrance aperture. Stray electrons that did leak through the analyzer shields were probably attracted to and absorbed on the lens elements and hemispheres, which were at high positive potentials, and did not reach the detector, which was shielded by its housing and an open-mesh grid in front of the cathode. The interaction region was well removed from slits and surfaces in the field of view of the analyzer. It was also helpful to use a "black" background for the field of view; this was accomplished by placing a conical trap opposite the entrance aperture so that stray electrons were less likely to bounce off the chamber wall in the field of view and thereby enter the analyzer. The various tests performed to verify that

stray electrons were eliminated are discussed in Sec. III B.

B. Electron and Atomic Beams

Primary electrons were generated in an electron gun and collected in a Faraday cup. Both were suspended from an arm driven by a worm gear that could be rotated from outside the vacuum system from 30° to 150° with respect to the input axis of the electron-energy analyzer.

To reduce stray-electron production, the normal oxide-coated cathode-grid structure of the 2BP1 oscilloscope electron gun was replaced by a tungsten-strip filament enclosed in a molybdenum cup "grid" structure. Both the grid structure and the filament were attached to a ceramic end plate in the electron-gun support tube. The filament was completely enclosed by the grid cup and ceramic end plate so that electrons emitted by the filament were either collected by the grid cup or emitted through a 0.25-mm-diam hole concentric with the axis of the electron-gun support tube. The filament was biased to the primary beam energy (100–2000 eV). Focus and beam current were adjusted with the use of resistive dividers from the filament bias supply to provide voltages for the grid and focus electrodes. The horizontal and vertical deflection plates in the electron gun were used for fine adjustment of the beam position and were driven symmetrically about ground potential. The electron beam was well focused, producing a 0.5-mm-diam spot on a phosphor screen at high energy. Beam currents used were typically between 10^{-8} and 3×10^{-7} A. The energy width was less than 0.5 eV, as determined by retarding potential analysis of the beam.

The gas sample was research-grade helium (less than 10 ppm impurities) introduced at a rate of 10^{18} atoms/sec into the ultrahigh-vacuum system (2×10^{-9} Torr base pressure) through a liquid-nitrogen trap. A known uniform distribution of the target gas over the interaction region could be produced by introducing the target gas through a port not in the line of sight of the interaction region (i.e., from behind the hemispherical analyzer). Target-gas pressures produced in this manner were, however, limited to pressures less than about 10^{-5} Torr because of high-voltage breakdowns. To increase the signal by about a factor of 10 the target gas was normally introduced from a 6-mm-diam copper tube 5 mm above the interaction region. This produced a target-gas density distribution that varied only slightly over the interaction region.

C. Data Acquisition and Normalization

For each primary-electron energy E_p, data were taken by setting the angle θ to one of nine equally spaced angles between 30° and 150° and repeatedly stepping the energy analyzer (10 msec/step) through 256 exponentially spaced energy settings ($4 \le E_s \le 200$ eV). The number of secondary electrons counted at each energy setting was accumulated in a 256-channel memory block of a small computer programmed to act as a multichannel scalar. These data were then converted to a count rate $R(E_p, E_s, \theta)$. After each data run, the primary energy was set to 100 eV, the angle was set to 90°, and the count rate of elastically scattered electrons R_{el} was recorded.

All data were then normalized to the 90°, 100-eV elastic scattering cross section σ_{el} (in cm^2/sr) as follows. Using the property of the analyzer that $\Delta E/E$ (called k below) is a constant, the cross section for production of secondary electrons of energy E_s at angle θ by primary electrons of E_p may be expressed as

$$\sigma(E_p, E_s, \theta) = G(E_s, \theta)\, R(E_p, E_s, \theta)$$
$$= \left(\frac{I_{100}}{I_p}\right)\left(\frac{R(E_p, E_s, \theta)}{R_{el}}\right)\frac{\sigma_{el}\sin\theta}{kE_s}\,, \qquad (2)$$

where I_{100}/I_p is the ratio of the beam currents used for elastic scattering and the ionization measurements. In using Eq. (2) we assumed that $\sigma(E_p, E_3, \theta)$ varied little over the bandpass of the analyzer ($\Delta E = kE_s$). The effective width used in calculating $\sigma(E_p, E_s, \theta)$ varies little over the bandpass of the analyzer. The effective width used in calculating k was such that the product of the width and the height of the elastic peak was equal to its integral over energy. The appropriateness of (2) is discussed in more detail below.

III. RESULTS AND DISCUSSION

A. Results

Data were recorded for primary energies between 100 eV and 2 keV, for secondary energies between 4 and 200 eV, and for angles of ejection between 30° and 150° with respect to the direction of the primary beam. The results for primary energies of 300, 500, 1000, and 2000 eV and for selected secondary energies are presented in Figs. 2 and 3. The 1000-eV data are displayed in a polar plot to emphasize the details of the angular distribution.

It can be seen from Figs. 2 and 3 that most of the secondary electrons produced have low energies (less than 25 eV) and that they are ejected relatively isotropically (the angular distribution is uniform within a factor of about 4). The most striking feature of the angular distributions is the peak in the data between 45° and 90°. This feature is interpreted as being due to the fact that the positive ion carries away relatively little momentum for the larger values of E_s. The peak was first observed and explained by Mohr and Nicoll.[8] Assuming that

no energy or momentum is transferred to the ion, one finds from energy and momentum conservation that the angle of the forward peak θ_{max} for a secondary electron of mass m and energy E_s produced by an ionizing particle of mass M and energy E_p is

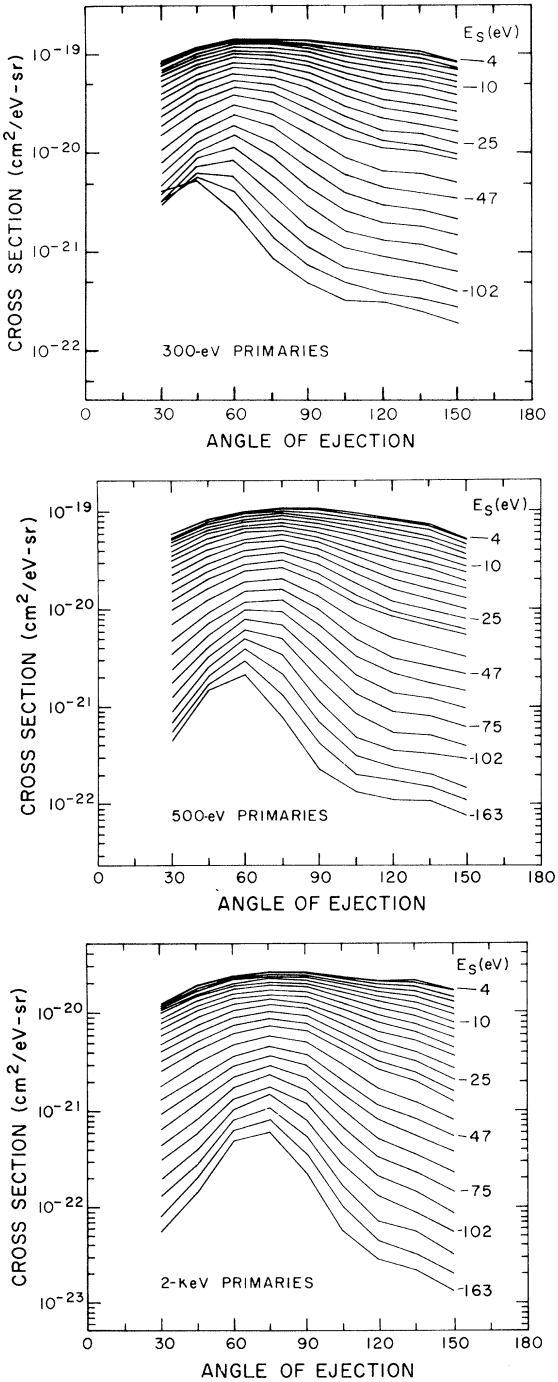

FIG. 2. Cross sections for the production of secondary electrons for selected values of secondary energy (E_s) and angle of ejection. The values of E_s shown are given by $E_s = 4 \times (\frac{65}{64})^{10(I-1)}$ eV, where $I = 1, 2, \ldots$.

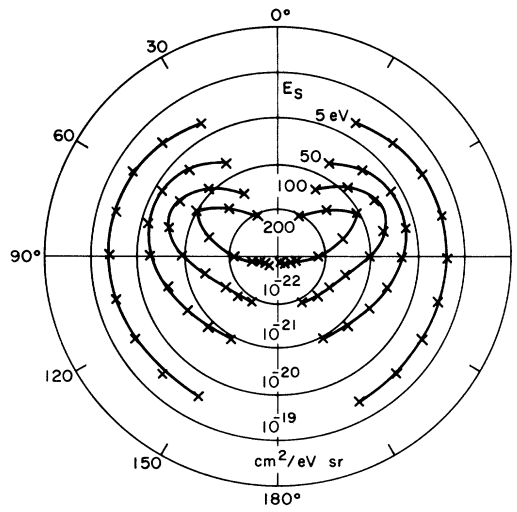

FIG. 3. Angular distribution of secondary electrons produced by 1000-eV primary electrons for selected secondary energies. Radial scale is logarithmic, with the center corresponding to a cross section of 10^{-23} cm^2/eV sr.

given by

$$\theta_{max} = \cos^{-1}\left[\frac{m+M}{2M}\left(\frac{ME_s}{mE_p}\right)^{1/2}\right] . \quad (3)$$

The experimental values of θ_{max} from the present results and for high-energy proton impact[13] follow Eq. (3) quite closely at higher values of E_s. The corresponding peak in the degraded primary angular distribution has also been observed.[15]

The spacing between the angular distribution curves in Fig. 2 for different secondary energies is almost independent of primary energy. This regularity is even more apparent in the energy distribution of secondary electrons and will be discussed below. In the range $30 < E_s < 35$ eV there is a slight irregularity in the otherwise uniform increase in spacing between curves of differing secondary energy. This is due to the autoionizing states of helium. The energy resolution of the present apparatus ($\Delta E \approx 3$ eV at 30 eV) is too broad to enable us to resolve the details reported previously.[16] Integrations of our data over all angles of ejection show that at $E_p = 100$ eV the total cross section for excitation of all of the autoionizing transitions is on the order of 10^{-19} cm^2, compared to 4×10^{-17} cm^2 for the total-ionization cross section. Similar ratios were found at all energies investigated.

B. Experimental Uncertainties

The three independent variables (E_p, E_s, and θ) were determined accurately, and uncertainties in their values were a negligible source of error. The dominant uncertainties in the results enter when the

observed counting rates are related to absolute cross sections, and arise from two sources: systematic effects, such as an angle- or energy-dependent sensitivity, which would mean that the assumed form of the sensitivity function G in Eq. (2) was in error, and spurious responses, which would produce counts unrelated to the cross section of the target at the energy and angle setting of the analyzer. The various possible sources of spurious counts will be discussed first.

With the electron gun turned off the counting rate (referred to below as dark current) was about 5 per sec (under normal operating conditions the primary current was set so the maximum counting rate was $\sim 5\times10^3$/sec). The dark current could be measured easily and a correction made. The remaining sources of counts gave a signal directly proportional to the primary beam current. These sources can usefully be divided into three categories: those which were independent of gas pressure, those which were linear in gas pressure, and those which depended nonlinearly on the pressure.

It was easy to test for those effects independent of pressure because the base pressure of the vacuum system ($< 10^{-8}$ Torr) was so much lower than typical operating pressures ($\sim 10^{-5}$ Torr except in the gas beam). Under normal operating conditions but with no target gas in the chamber the count rate was negligible.

Background counts linear in target density could be caused by three general mechanisms: (i) Although the electron analyzer was designed to transmit only electrons in a rather narrow energy band, it was possible that electrons at other energies or photons generated spurious counts. (ii) Scattered electrons could produce secondaries at the walls, which could then enter the analyzer. (iii) Secondaries generated on surfaces could get to the detector after scattering from the gas. A series of tests was conducted to estimate the sizes of these effects:

(i) A shielded test filament was placed in the interaction region and biased to an energy E_b so that the field of view of the analyzer was filled by a shower of relatively monoenergetic electrons. The observed spectrum was appropriately sharply peaked at E_b, and the count rate was negligible when the analyzer energy was significantly different from E_b. It was concluded that the probability that a recorded count would be caused by an electron with energy far outside the bandpass of the analyzer was less than 10^{-5}. Another possibility was that photoelectrons were produced in the analyzer by x rays generated by the primary beam or by far-ultraviolet emissions from He. The first is very unlikely because few of the primary electrons were scattered at large enough angles to impact on a surface in the field of view of the analyzer. The dominant emissions in He are at photon energies less than 50 eV, which is less than the positive potentials on the lens elements except at the very lowest energy settings. Thus the resulting photoelectrons would not have enough energy to escape from the lens elements and pass through the grounded grid in front of the detector. As a test for photoelectrons, the first lens element (the one most likely to produce photoelectrons) was run at a negative voltage higher than the primary energy so that electrons coming through the entrance aperture would be repelled out of the analyzer and photoelectrons coming from the lens would be accelerated into the analyzer. No signal was observed under these conditions.

(ii) By using the steering plates in the gun, the electron beam could be deflected out of the Faraday cup. Thus, with no gas flow it was possible to simulate the background from solid surfaces which would be produced if the entire beam were scattered by the gas target. The result was a spectrum of electrons about equal to the signal with gas flow at low energies but falling more rapidly toward high energies. With a total elastic scattering cross section of 10^{-16} cm^2 we calculate that a fraction of the primary beam smaller than 10^{-4} was scattered out of the Faraday cup in normal operation; consequently, the counting rate from this cause was negligible.

(iii) Moving the beam out of the Faraday cup, increased the counting rate due to scattering solely from surfaces by a factor greater than 10^3. It is reasonable to assume that background effects due to scattering from both a solid and the target gas would be increased by a similar factor. The result of turning on the gas in the presence of this high artificial background from surfaces was an increase in counting rate which could be attributed almost entirely to the normal signal from the gas alone. Thus, we conclude that with the beam in the Faraday cup a negligible fraction of the primary electrons which pass through the gas beam cause spurious counts by any mechanism. There remains the possibility that counts may be caused by secondaries generated in the electron gun and scattered into the analyzer by the gas. These low-energy electrons would most likely result from inelastic scatterings of primary electrons on the edges of defining apertures in the gun. Some indirect evidence suggests that this did not occur. With the energy of the primary beam less than 200 eV the observed spectrum includes the energy-degraded primaries and an elastic peak. Since in helium an inelastic collision cannot result in an energy loss less than 19 eV, the counting rate due to gas interactions is zero when the analyzer is set just below the elastic peak. In this window, where primary electrons which collided with apertures would be expected to occur, the observed counting rate was less than 10^{-4} times the counting rate at the elastic peak. In addition, during the course of

testing secondary spectra were recorded for several different geometrical arrangements of the gun and for both positive and negative voltages on the focus electrode (the only one not at either ground or cathode potential), with no observable change in results.

Counts caused by processes involving two scatterings from gas molecules can in principle be distinguished by examination of the gas density dependence. The density was raised a factor of 3 above the normal operating pressure with no observable change in relative counting rates. Actually most of the potential errors due to multiple scattering were eliminated by the above tests for a background linear in gas density.

It is necessary to consider the appropriateness of the function G, which relates the observed counting rates to the absolute cross sections. That is, it remains to be determined to what extent Eq. (2) is accurate in describing the efficiency of collection.

At a primary energy of 100 eV the energy width of the analyzer was much larger than the energy width of the primary beam, but the resolution was high enough to separate the elastically scattered electrons from those inelastically scattered. Thus it was possible to eliminate poorly known factors, such as the target-gas density and geometrical factors, by expressing the inelastic cross sections in terms of the elastic cross section according to Eq. (2). Several aspects of the uncertainties in this normalization need to be discussed separately: (i) The uncertainties in $\sigma(E_p, E_s, \theta)$ relative to $\sigma(E_p,$ 100 eV, 90°). (ii) The uncertainties in $\sigma(E_p,$ 100 eV, 90°) relative to σ_{el}(100 eV, 90°). (iii) The uncertainties in σ_{el}(100 eV, 90°).

(i) It was assumed that at angles away from 90° the sensitivity of the analyzer was increased by the (approximately correct) factor $1/\sin\theta$ because of the increased length of the interaction region in the field of view of the analyzer. It is possible, however, that defocusing and vignetting reduced the transmission at large angles. Also, the effect of any variations in the gas density along the beam would become more important. To verify that the target-gas density produced by introducing the target gas directly above the interaction region was nearly uniform, angular distributions or secondary electrons produced this way were compared with a more uniform distribution obtained by introducing the gas from behind the hemispherical analyzer. The ratios of secondary electrons of a fixed energy (normally 20 eV) at a fixed angle produced by these two methods was found to vary as much as 20% between 30° and 90° (and between 90° and 150°). An attempt was made to use the published elastic scattering cross sections as a function of angle for 100-eV primaries on helium[17] and 300-eV primaries on N_2[18] to calibrate the angular response of the analyzer. The uncertainty in the angular acceptance of the analyzer made detailed comparison inconclusive, but assuming the nominal 15° angular acceptance and a uniform target distribution the present results were consistent with the previous measurements of these differential cross sections. In view of the agreement with elastic scattering cross sections and the reproducibility of the results with different aperture and exit-slit sizes, the uncertainty in the ratios of cross sections with the same primary and secondary energies and at angles of 30° and 150°, relative to 90°, was estimated to be 25%. Ratios at more closely spaced angles are less uncertain.

The energy analyzer was operated in a mode such that, to first order, its transmission was independent of E_s. The lack of dependence of the analyzer transmission on the energy of the electron being analyzed was verified by recording spectra produced by a shielded, emission-limited tungsten filament in the interaction region with various bias voltages applied to the filament. The widths of the spectra showed that the energy resolution was indeed proportional to energy if the energy width of the primary beam (~ 0.5 eV) was taken into account. The filament was also used to calibrate the energy scale to an accuracy of about 3%. By measuring the width of the elastic scattering peak from helium we verified that the energy resolution did not vary with angle. These data showed that the transmission of the analyzer and sensitivity of the channel electron multiplier were constant to within 10% for the extremes of the energy range. For values of E_s more closely spaced the uncertainty is correspondingly less.

Changing the primary-electron energy can have little effect on relative values of $\sigma(E_p, E_s, \theta)$ for different values of θ except through stray electric fields. A test was made for the effects of electric fields when the test filament was in place. No effect was observed. Shielding of the analyzer elements was tested by observing the deflection of the primary-electron beam as voltages applied to the analyzer were changed; the deflections observed were negligible.

(ii) The uncertainties in $\sigma(E_p,$ 100, 90°) relative to σ_{el}(100, 90°) arise from possible changes in the gas density between two successive determinations, and possible changes in the position or shape of the electron beam as the primary energy is changed. The electron-beam position could be determined by noting the potentials required on the steering electrodes to place it in the center of the Faraday cup; the position did not depend on primary energy for $E_p \geq 100$ eV. The shape of the beam could not be readily monitored; however, so long as its width was less than the width of the image of the exit slit, the shape made little difference. Uncertainties due to these sources were probably less than 10%.

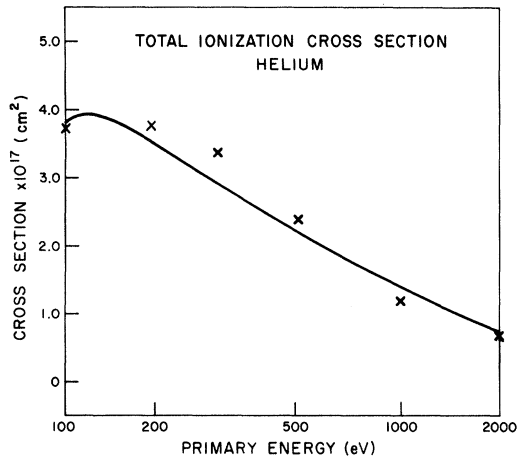

FIG. 4. Total ionization cross section. Crosses, present results; solid line, results of Smith (Ref. 20).

(iii) The value of $\sigma_{el}(100, 90°)$ used in reporting these data was 2.0×10^{-18} cm^2/sr. This value was chosen to be consistent with previous experimental and theoretical determinations.[17] We believe that the adopted value may be in error by as much as 20%. When a more reliable value becomes available the appropriate adjustment should be made in $\sigma(E_p, E_s, \theta)$.

In addition to the tests described above, a number of consistency checks were performed. Spectra were recorded with various sizes of entrance apertures and exit slits, with slight perturbations in the potentials applied to the electron-lens and -gun elements, with different primary currents and gas flow rates, and with different sizes and positions of the gas effuser. These changes in conditions changed the results by no more than about 10%.

Finally, we should note that the time required to reduce statistical uncertainties to a negligible level[19] was several hours for a complete data run at a particular energy. During this period drift in the gas flow and the primary current, which were not perfectly regulated, as well as possible changes in unmonitored quantities such as the external magnetic field, could have introduced other systematic errors in the results. The conclusion reached from consistency checks of a great many trial runs was that discrepancies as large as 10% arose because of failure to control adequately all the relevant variables.

Also of interest are uncertainties in the singly differential cross section obtained by integrating the data over angle with the use of Eq. (1). In performing this integration to obtain secondary electron distribution, the solid-angle factor $\sin\theta$ greatly reduced the contribution of data at extreme forward and backward angles; consequently, the contribution of the uncertainty of the data at these angles to uncertainty in the secondary energy distribution $\sigma(E_p, E_s)$ was reduced. Similarly, the extrapolation of the data to smaller and larger angles was relatively unimportant, being over only 15% of the total solid angle. The error introduced in the extrapolation to smaller angles was greatest at the largest secondary energies or near $E_s \approx \frac{1}{2}(E_p - I)$, where most of the secondaries are ejected at about 45°. A test of the sensitivity of $\sigma(E_p, E_s)$ to the uncertainties of the doubly differential cross section was made by omitting the $\sin\theta$ factor in the integral, thus making the contribution from the extreme forward and backward angles relatively more important. For 500-eV primaries, this caused a change of less than 10% in the relative values of $\sigma(E_p, E_s)$ for all values of E_s.

A conservative estimate of the experimental uncertainties in $\sigma(E_p, E_s)$ is that the ratio $\sigma(E_p, 4\text{ eV})/\sigma(E_p, 200\text{ eV})$ is accurate to 25%. This uncertainty comes from possible systematic dependence on angle (10%) and energy (10%), and other effects (discussed above). Ratios at more closely spaced intervals are more accurate.

As an independent check of the normalization procedure, the above singly differential cross sections were integrated over all secondary energies (assuming that the cross section was constant below 4 eV) to obtain total ionization cross sections for each primary energy. The results of these integrations are compared with the total ionization cross-section measurements of Smith[20] in Fig. 4. The agreement is within the experimental uncertainties of the present results.

C. Prior Results

As noted in the Introduction, relatively little experimental work has been devoted to the study of secondary electrons. In the 1930's Mohr and Nicoll[8] reported energy and angular distributions for electrons from helium with several primary energies, and Goodrich[9] gave similar data for 100-eV primaries. Both of these measurements were done without the benefit of particle counters and in consequence rather high gas densities were required. Both researches were concerned more with investigating qualitative features of the data than with trying to produce accurate absolute results. Mohr and Nicoll did not determine an absolute normalization of the data, and Goodrich concluded that because of some problem with his pressure-measuring system his results were undoubtedly too low. Samples of the data from these measurements are displayed in Figs. 5 and 6. The significant differences between these data and our results are that Mohr and Nicoll found a relatively large number of electrons in the backwards hemisphere, and both previous experiments found many more electrons in the forward direction ($\theta < 60°$) than we did. A detailed

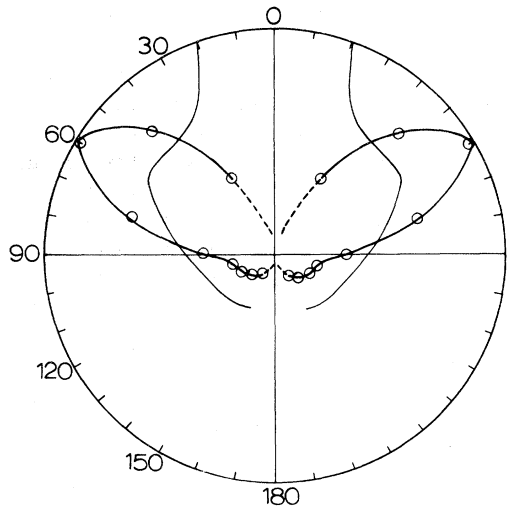

FIG. 5. Angular distribution of 50-eV electrons ejected from helium by 200-eV primary electrons. Circle line, present results; dashed line, extrapolation of present results; solid line, data of Mohr and Nicoll (Ref. 8). The present results are normalized to their maximum; the Mohr and Nicoll results are normalized to their value at 20°.

analysis of their measurements to find the cause of discrepancy is not possible; however, based on the following considerations we believe their reliability is rather low. The cross sections for both elastic and inelastic scattering are largest in the forward direction and decrease rather rapidly with angle. This creates the possibility of a large-angle scattering occurring through two smaller-angle scatterings. The gas density used by Goodrich was sufficiently high to have caused such nonlinearities. Mohr and Nicoll used comparable gas densities but did not report in detail the effects of changing the density. It is possible that the excess electrons observed in the backward hemisphere by Mohr and Nicoll were due to a gas-dependent background. The current arriving at their detector under these circumstances must have been very small. In any case, except for the forward peak at low secondary energies, we agree with the qualitative conclusions of these early authors.

More recently Ehrhardt *et al.*[10] and Oda *et al.*[11] reported some measurements of relative cross sections. Ehrhardt *et al.* concentrated primarily on the degraded primary spectrum, and presented only a few secondary spectra. These spectra cannot be compared directly with ours but do show the same qualitative features. Oda *et al.* showed angular distributions for $E_p = 500$ eV and $E_s = 27.5$ and 43.5 eV at angles between 15° and 105°, which they normalized to a binary-encounter theory. The absolute values they obtained are somewhat higher than ours, but never by more than 25%; agreement is therefore satisfactory.

Previously published calculations have been based on either the Born approximation or the binary-encounter approximation. In most of the published Born-approximation calculations of electron-impact ionization of helium, only the energy distributions have been reported. The results of the one calculation[21] in which both energy and angular distributions of secondary electrons were predicted agree only qualitatively with the present results. This is not surprising, as a hydrogenic wave function, which does not describe the helium atom very well,[22] was used. Published calculations based on the binary-encounter theory also have generally been for the energy distribution only.[23] Moreover, the angular distributions of secondary electrons predicted by the binary-encounter theory are unrealistic in that the number of secondary electrons ejected into the backward hemisphere is greatly underestimated.[24] And, finally, in neither of the above calculations[21,23] were the effects of electron exchange taken into account.

Theories of ionization predict that at high energies the total ionization cross section depends only on the velocity of the particle and the magnitude of its charge. This has been verified experimentally for total ionization cross sections for velocities greater than those of 2-MeV protons or 1-keV electrons.[25] Even though the total ionization cross sections are the same at velocities greater than these, the differential ionization cross sections are not necessarily identical because of the differences in the masses of the ionizing particles [cf. Eq. (3)]. For lower proton energies, an additional peak is observed in the angular distribution at forward angles.[12,26] This has been explained in

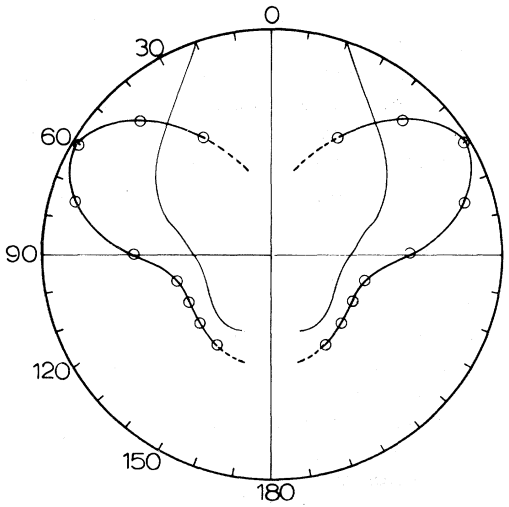

FIG. 6. Angular distribution of 23-eV electrons ejected from helium by 100-eV electrons. Solid line represents results of Goodrich (Ref. 9); other symbols and normalization are the same as in Fig. 5.

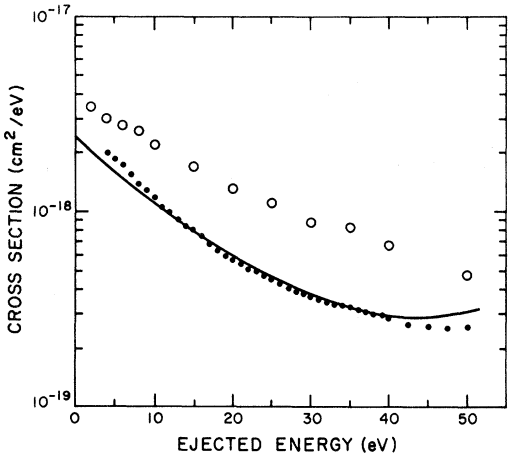

FIG. 7. Cross section for production of secondary electrons by proton and electron impact. Circle line, 200-keV proton impact, measured by Rudd *et al.* (Ref. 12); dotted line, 113-eV electron impact, present results; solid line, 113-eV electron impact, Born-exchange calculation (normalized to the present results at $E_s = 15$ eV) by Sloan (Ref. 28). Velocity of 200-keV protons is the same as that of 113-eV electrons.

terms of the Coulomb attraction between the ionizing proton and the ejected electron.[27] There is one more difference between electron and proton impact, which arises from the indistinguishability of the two outgoing electrons in electron-impact ionization. The consequences of this effect can be best illustrated by the use of the secondary-electron energy distributions discussed below.

D. Energy Distributions of Secondary Electrons

We have derived energy distributions (singly differential cross sections) by integrating the doubly differential cross sections over angle using the procedure described in Sec. II B. Figure 7 shows the results of this integration for 113-eV electrons and protons of comparable velocity (200 keV). Also shown is a Born-approximation calculation, including the effects of electron exchange.[28] Most of the difference in the magnitude of the proton and electron impact cross sections can be explained by the extra forward peak in the proton data, which was discussed above. The difference in shapes can be explained in terms of the effects of electron exchange. The relative magnitude of the exchange effect is best seen by comparing the observed cross section with the quantum-mechanical cross section for the scattering of a nonrelativistic electron from a stationary free target electron, for which Mott has given the formula[29]

$$\sigma_M(E_p, E_s) = \frac{\pi e^4}{E_p}\left(\frac{1}{E_s^2} + \frac{1}{(E_p - E_s)^2} - \frac{\cos\delta}{E_s(E_p - E_s)}\right). \quad (4)$$

Here the first term is the classical Coulomb scattering term for the target electron, the second term is that for the incident electron, and the third term is a quantum-mechanical term resulting from the interference of the outgoing electrons. For present purposes $\cos\delta$ can be set to unity. This formula has been shown to be applicable for secondary energies of several keV and for primary energies as low as 20 keV.[30] At lower primary and secondary energies, one might expect that the effects of binding of the target electrons would be more important, and consequently that the formula would no longer apply.

The ratios of the measured helium cross sections to those given by the Mott formula are plotted in Fig. 8. Data for E_s above 200 eV for the 1-keV primaries were taken with a manually scanned power supply, rather than with the automated equipment used for the others, and are not as accurate because of possible drifts during the data taking process and because of the small signal levels involved. For primary energies greater than 300 eV and secondary energies greater than 50 eV, it is seen that the curves approach, within experimental error, the expected value of 2.0 (the number of "free" electrons in the target). If the electron interference term were not present these ratios would fall to about 1.0 near $\frac{1}{2}E_p$.

The divergence of $\sigma_M(E_p, E_s)$ at $E_s = 0$ is a consequence of the assumption that the electrons are free. In ionization the low-energy ejected electron must leave in the field of a positive ion. It is tempting to modify the Mott formula to correct for this effect[23] and some empirical corrections result in a rather good match of the formula with the data. In general, however, it is clear that the interaction

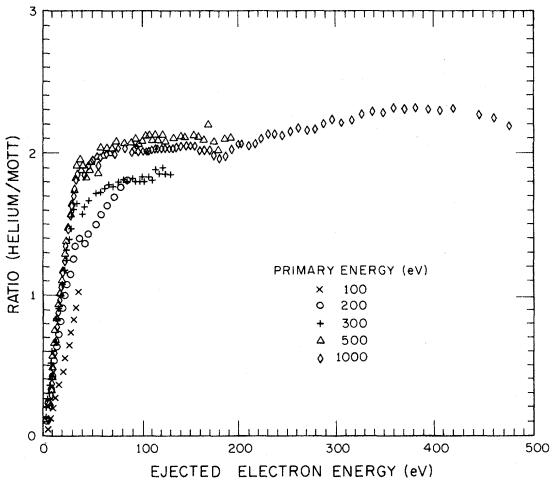

FIG. 8. Ratios of the observed cross sections for production of secondary electrons to those predicted by the Mott formula.

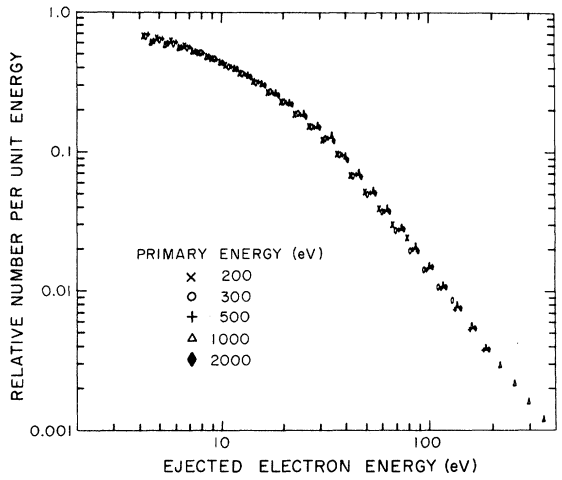

FIG. 9. Secondary-electron energy distributions normalized at $E_s = 75$ eV to the Mott formula.

leading to low-energy secondaries is not due to a binary encounter of one electron with another. The principal appeal of the binary-encounter model is that it does not require knowledge of the atomic wave function and can therefore be applied to more complicated systems than can the Born approximation. In the case of helium the Born approximation has been worked out for reasonable wave functions and the calculated cross sections agree well with the data (see Fig. 7 and Ref. 1).

As discussed above, the experimental values of $\sigma(E_p, E_s)$ are consistent with the hypothesis that they are twice those given by the Mott formula for 50 eV $< E_s < \frac{1}{2}E_p$ and $E_p > 300$ eV. Some of the trends with E_p can be more easily examined if the data are renormalized to the Mott formula. Plotted in Fig. 9 are values of $E_p\,\sigma(E_p, E_s)$ with $\sigma(E_p, E_s)$ normalized so that $\sigma(E_p, 75\text{ eV}) = 2\sigma_M(E_p, 75\text{ eV})$. For purposes of the present discussion the absolute scale is not relevant, and a convenient relative scale for the energy distributions was used in Fig. 9. The principal conclusion to be drawn from Fig. 9 is that the shapes of the curves for different E_p are approximately the same. A second conclusion is that $\sigma(E_p, E_s)$ varies approximately as E_p^{-1} for $E_p > 200$ eV. (The renormalization of Fig. 9 is within the stated uncertainties of the experimentally derived normalization as can be seen from Fig. 8.) As noted above there is good reason to believe the Mott formula is applicable where both E_s and E_p are much larger than the ionization potential.

It is known from the Bethe theory,[31] which has been verified by experiment,[20] that the total ionization cross section varies as $E_p^{-1}\ln(E_p)$ for large (nonrelativistic) E_p. Thus we are led to expect the curves of Fig. 9 to diverge on the low-energy side. That they do not may be due to the inaccuracy of the normalization used. (The experimentally derived normalization is less consistent.) But it may also be due to the fact that the data do not extend to low enough energy to show the effect. It is worth noting that the logarithmic dependence is phenomenologically due to the effects of distant encounters, and that these would be expected to yield predominantly low-energy electrons.[32]

IV. SUMMARY

Energy and angular distributions for electrons ejected upon electron-impact ionization of helium have been presented for a wide range of parameters. It is our hope that these data will be useful in energy-degradation studies and will provide better tests of ionization theory than do measurements of total ionization cross section.

We have compared our data with several types of previous results. Electron-impact measurements made in the 1930's (which have been largely ignored in the literature) did not completely agree with ours; we have discussed reasons for believing that some of these early results were, in part, invalid. Agreement with more recent measurements (with a more limited range of energies and angles than reported here) was considerably better. We also compared our electron-impact results with results with recent proton-impact measurements and pointed out three qualitative differences which could be explained by the difference in impacting particles. One of these differences is the result of the indistinguishability of the incident and ejected electrons; we demonstrated the effects of the exchange of the two electrons by integrating the doubly differential cross sections over angle and comparing the observed energy spectrum with that predicted by the quantum-mechanical Mott formula for free-electron–free-electron scattering, which includes exchange. The helium results agreed with the Mott formula down to surprisingly low energies of the primary (300 eV) and the secondary (50 eV) electrons.

ACKNOWLEDGMENTS

The success of this work is in large part due to the assistance and advice of a number of our colleagues at JILA. We would like to thank G. H. Dunn, G. C. Chamberlain, L. J. Kieffer, and A. V. Phelps for their comments on the manuscript.

*Research supported by the Advanced Research Projects Agency and the Department of Defense, and was monitored by U. S. Army Research Office-Durham, Box CM, Duke Station, N. C. 27706, under Contract No. DA-31-124-ARO-D-139.

†Present address: Deutsches Elektronen-Synchrotron,

Hamburg, Germany.

‡Staff Member, Laboratory Astrophysics Division, National Bureau of Standards.

§Present address: E. O. Hulbert Center for Space Research, Naval Research Laboratory, Washington, D.C. 20390.

[1]W. K. Peterson, C. B. Opal, and E. C. Beaty, J. Phys. B 4, 1020 (1971).

[2]A more complete discussion of the experimental procedure is available in W. K. Peterson, Ph.D. thesis (University of Colorado, 1971) (unpublished), and the complete tabulation of all of the data for helium and 14 other gases is in University of Colorado JILA Report No. 108 (unpublished); also see C. B. Opal, W. K. Peterson, and E. C. Beaty, J. Chem. Phys. 55, 4100 (1971).

[3]H. R. Moustafa Moussa and F. J. DeHeer, Physica 36, 646 (1967).

[4]L. J. Kieffer and G. H. Dunn, Rev. Mod. Phys. 38, 1 (1966).

[5]H. Ehrhardt, M. Schulz, T. Tekaat, and K. Willmann, Phys. Rev. Letters 22, 89 (1969); H. Ehrhardt, K.-H. Hesselbacher, and K. Willmann, in *Proceedings of the Sixth International Conference on the Physics of Electronic and Atomic Collisions: Abstracts of Papers* (MIT, Cambridge, Mass., 1969), p. 217.

[6]S. M. Silverman and E. N. Lassettre, J. Chem. Phys. 40, 1265 (1964); E. N. Lassettre, Can. J. Chem. 47, 1733 (1969).

[7]See the calculation of Peach in H. S. W. Massey, E. H. S. Burhop, and H. B. Gilbody, *Electronic and Ionic Impact Phenomena*, 2nd ed. (Clarendon, Oxford, England, 1969), p. 489.

[8]C. B. O. Mohr and F. H. Nicoll, Proc. Roy. Soc. (London) A144, 596 (1934).

[9]M. Goodrich, Phys. Rev. 52, 259 (1937).

[10]H. Ehrhardt, K.-H. Hesselbacher, K. Jung, M. Schulz, T. Tekaat, and K. Willmann, Z. Physik 244, 254 (1971).

[11]N. Oda, F. Nishimura, and S. Tahira, in *Proceedings of the Seventh International Conference on the Physics of Electronic and Atomic Collisions: Abstracts of Papers* (North-Holland, Amsterdam, 1971), p. 875.

[12]M. E. Rudd, C. A. Sautter, and C. L. Bailey, Phys. Rev. 151, 20 (1966).

[13]L. Toburen, Phys. Rev. A 3, 216 (1971); in *Proceedings of the Seventh International Conference on the Physics of Electronic and Atomic Collisions: Abstracts of Papers* (North-Holland, Amsterdam, 1971), p. 1120.

[14]K. R. Spangenberg, *Vacuum Tubes* (McGraw-Hill, New York, 1948); E. M. Purcell, Phys. Rev. 54, 818 (1938); C. E. Kuyatt and J. A. Simpson, Rev. Sci. Instr. 38, 103 (1967).

[15]See, for example, A. L. Hughes and M. M. Mann, Phys. Rev. 53, 50 (1938).

[16]N. Oda, F. Nishimura, and S. Tahira, Phys. Rev. Letters 24, 42 (1970); H. Suzuki, A. Konishi, M. Yamamoto, and K. Wakiya, J. Phys. Soc. Japan 28, 534 (1970).

[17]K. G. Williams, in *Proceedings of the Sixth International Conference on the Physics of Electronic and Atomic Collisions: Abstracts of Papers* (MIT, Cambridge, Mass., 1969), p. 735; S. Westin, Kgl. Norske Videnskab. Selskabs Skirfter 2, 1 (1946); S. Werner, Proc. Roy. Soc. (London) A139, 113 (1933); A. L. Hughes, J. H. McMillen, and G. M. Webb, Phys. Rev. 41, 154 (1932); R. W. Labahn and J. Callaway, Phys. Rev. A 2, 366 (1970); L. Vriens, C. E. Kuyatt, and S. R. Mielczarek, Phys. Rev. 170, 163 (1968).

[18]J. P. Bromberg, J. Chem. Phys. 52, 1243 (1970).

[19]For most of the cross sections reported here more than 1000 counts were recorded, corresponding to a statistical uncertainty of 3%. For cross sections less than about 5×10^{-22} cm^2/eV sr, however, fewer counts were recorded, and the uncertainty associated with these cross sections is greater.

[20]P. T. Smith, Phys. Rev. 36, 1293 (1930).

[21]H. S. W. Massey and C. B. O. Mohr, Proc. Roy. Soc. (London) A140, 613 (1933).

[22]See, for example, W. F. Miller, and R. L. Platzman, Proc. Phys. Soc. (London) A70, 299 (1957).

[23]See, for example, A. Burgess and I. C. Percival, in *Advances in Atomic and Molecular Physics*, edited by D. R. Bates and I. Esterman (Academic, New York, 1968), Vol. 4, p. 109.

[24]T. F. M. Bonsen and L. Vriens, Physica 47, 307 (1970).

[25]See, for example, E. W. McDaniel, *Collision Phenomena in Ionized Gases* (Wiley, New York, 1964), p. 182.

[26]G. B. Crooks and M. E. Rudd, Phys. Rev. Letters 25, 1599 (1970).

[27]A. Salin, J. Phys. B 2, 631 (1969); J. Macek, Phys. Rev. A 1, 235 (1970).

[28]I. H. Sloan, Proc. Phys. Soc. (London) 85, 435 (1965).

[29]N. F. Mott, Proc. Roy. Soc. (London) A126, 259 (1930).

[30]E. J. Williams, Proc. Roy. Soc. (London) A128, 459 (1930).

[31]See, for example, H. A. Bethe and J. Ashkin, in *Experimental Nuclear Physics*, edited by E. Segrè (Wiley, New York, 1953), p. 166; M. Inokuti and Y.-K. Kim, Phys. Rev. 186, 100 (1969).

[32]M. Inokuti, Rev. Mod. Phys. 43, 297 (1971).